Lasers and Light vol. 8 no. 1 pp 15-29 (1997)
Kugler Publications, Amsterdam/New York

A comparison of laser-induced retinal damage from infrared wavelengths to that from visible wavelengths

Joseph A. Zuclich[1], Steven T. Schuschereba[2], Harry Zwick[2], Stephen A. Boppart[3], James G. Fujimoto[3], Frank E. Cheney[4] and Bruce E. Stuck[2]
[1]TASC, San Antonio, TX; [2]US Army Medical Research Detachment, Brooks AFB, TX; [3]Massachusetts Institute of Technology, Cambridge, MA; [4]Optical Radiation Division, Armstrong Laboratory, Brooks AFB, TX; USA

Keywords: infrared laser, retina, ocular damage, SLO, histopathology

Abstract

Corneal, lenticular, and retinal damage have been observed following exposures to a laser emitting in the near-infrared wavelength range (Nd:YAG, 1.318 μm). Ocular damage thresholds are much higher than for visible wavelengths. However, it was found that infrared (IR) exposures may result in multiple damage sites throughout the ocular medium and retina; *that exposure sites which initially appear to be unaffected* may reveal slowly developing (days or longer) degeneration; and that late inflammatory responses may ultimately spread to areas of tissue not directly irradiated by the laser.

The nature of tissue degeneration following IR laser exposure is examined and compared to that following visible wavelength laser exposures *using three approaches: histopathology, scanning laser ophthalmoscopy, and optical coherence tomography. Each approach is shown to reveal unique aspects of the IR laser-tissue interaction when contrasted with effects induced by visible wavelengths.*

Introduction

Recent developments in laser technology have yielded a variety of powerful infrared (IR) laser sources, many of which fall in the wavelength range broadly categorized as 'eye-safe'. Used in this context, the terminology is frequently divorced from its original intent as a relative descriptor meant only to convey the fact that ocular damage thresholds are significantly higher for 'eye-safe' wavelengths than for elsewhere in the visible and IR spectra.

Transmission spectra of the ocular components (cornea, aqueous, lens, and vitreous) of the primate eye are plotted in Figure 1[1]. From this illustration, it can be seen that transmission through each component (and, therefore, transmission to the retina) is high for visible wavelengths and only begins to drop significantly for IR wavelengths above ~1.1 μm, where water absorption becomes appreciable. In the far-IR, the composite absorption of the ocular components is such that virtually no incident radiation is transmitted to the retina. In the near-IR, absorption of incident radiation is distributed across the ocular components and, depending upon the precise exposure parameters, damage may be induced in one or more of the cornea, lens, and retina/choroid.

The simultaneous induction of laser-induced damage in several tissues is perhaps best understood by schematizing the distribution of energy absorption through the ocular medium. This is done in Figure 2 which compares the absorption of 0.514-μm argon laser radiation (Fig. 2a) to that for the 1.318-μm Nd:YAG laser emission used in this study (Fig. 2c). Distance into the eye is meas-

Address for correspondence: Joseph A. Zuclich, PhD, TASC, 4241 Woodcock Drive, Suite B-100, San Antonio, TX 78228, USA

coherence tomography. Opt Engineer 34:701, 710, 1995
10. Fujimoto JG, Brezinski ME, Tearney GJ, Boppart SA, Bouma B, Hee MR, Southern JF, Swanson EA: Biomedical imaging and optical biopsy using optical coherence tomography. Nature Med 1:970-972, 1995
11. Pan Y, Birngruber R, Rosperich J, Engelhardt R: Low-coherence optical tomography in turbid tissue: theoretical analysis. Appl Opt 34:6564-6574, 1995
12. Schuschereba ST, Bowman PD, Vargas JA, Johnson TW, Woo FJ, McKinney L: Myopathic alterations in extraocular muscle of rats subchronically fed pyrodostigmine bromide. Toxicol Pathol 18:103-123, 1990
13. Karnovsky MJ: A formaldehyde-glutaraldehyde fixative of high osmolality for use in electron microscopy. J Cell Biol 27:137A-138A, 1965
14. Frisch GD, Beatrice ES, Holsen RC: Comparative study of argon and ruby retinal damage thresholds. Invest Ophthalmol 10:911-919, 1971
15. Majno G, Joris I: Apoptosis, oncosis and necrosis: an overview of cell death. Am J Pathol 146:3-15, 1995

duced lesions are generally observed shortly following exposure and, within hours, *stabilize so that no further changes in appearance are noted, save for the gradual fading in* reflectivity over a period of months. In contrast, the IR retinal lesions were first detected only upon re-examination of subjects on the day following exposure, and thereafter. This delay time in the formation of observable damage is suggestive of a damage mechanism such as thermally-induced programmed cell death or apoptosis[15]. Funduscopically, the IR lesions reached maximum intensity at ~48 hours postexposure. *Pathological evaluation at that time revealed the presence of* numerous inflammatory cells in the vitreous and at the ILM interface directly above the IR retinal lesion. The suggestion is made that this finding is a prognosticator of the late inflammatory response which expressed itself as the large, irregularly shaped opacity found at a 1.318-μm exposure site at two months postexposure (Fig. 9). SLO observation of the two-month inflammatory response indicated strong involvement of the inner retina. Continued monitoring of the subject showed that the inflammatory response gradually cleared during the following month, so that by three months postexposure the underlying circular lesion was again visualized.

In summary, the IR wavelength studied (1.318 μm) defines the upper limit of wavelength where there is still sufficient transmission through the ocular medium to affect the retina of the eye[1,2]. Because such a large percentage of the incident IR laser radiation is absorbed by the ocular medium, and because that radiation which reaches the retina is not focused to as small an image size nor absorbed there as strongly as visible wavelengths, a very high dose of IR must be incident at the cornea to cause detectable funduscopic damage to the retina. Thus, the term 'eye-safe' has been applied even to higher power lasers in this segment of the IR wavelength region. However, it should be emphasized that applying the term 'eye-safe' to a given wavelength or wavelength band without regard to the laser power level and other beam characteristics, is inconsistent with published laser safety standards. Further, we report several observations which belie the 'eye-safe' terminology. First, a threshold IR lesion involves a volume of retinal tissue many orders of magnitude greater than that affected by a threshold-visible laser exposure and, hence, represents a more serious injury. Second, the usual threshold definition of a minimal visible lesion detected by funduscopic observation is not appropriate for the IR wavelength, since the monochromatic SLO imaging can detect retinal effects induced by significantly lower exposure doses. These observations, together with the delayed inflammatory responses observed histologically (Fig. 10) and funduscopically (Fig. 9), suggest that serious visual consequences may develop following a 'threshold' IR laser exposure.

Acknowledgements

The research reported here was supported by the US Army Medical Research Detachment and the Optical Radiation Division, Occupational and Environmental Health Directorate, USAF Armstrong Laboratory, Brooks AFB, TX, under Contract F33615-92-C-0017 (TASC), let by the USAF. SAB and JGF received support from the Air Force Office of Scientific Research (#2312AA-92AL014). The work was conducted at Brooks AFB, TX.

References

1. Maher EF: Transmission and absorption coefficients for ocular media of the rhesus monkey. SAM-TR-78-32, 1978
2. Boettner EA: Special transmission of the eye. University of Michigan, Final Report, USAF Contact F41(609)-2966, 1967
3. Zuclich JA, Gagliano DA, Cheney F, Stuck BE, Zwick H, Edsall P, Lund DJ: Ocular effects of penetrating IR laser wavelengths. SPIE 2391:112-125, 1995
4. Webb RH, Hughes GW, Delori FC: Confocal scanning laser ophthalmoscope. Appl Opt 26:1492-1499, 1987
5. Zwick H, Gagliano DA, Stuck BE, Lund DJ: Comparison of solar and laser macular retinal injury using SLO spectral imaging. SPIE 2134B:54-63, 1994
6. Huang D, Swanson EA, Lin CP, Schuman JS, Stinson WG, Chang W, Hee MR, Flotte T, Gregory K, Puliafito CA, Fujimoto JG: Optical coherence tomography. Science 254:1178-1181, 1991
7. Hee MR, Izatt JA, Swanson EA, Huang D, Schuman JS, Lin CP, Puliafito CA, Fujimoto JG: Optical coherence tomography of the human retina. Arch Ophthalmol 113:326-332, 1995
8. Puliafito CA, Hee MR, Lin CP, Peichel E, Schuman JS, Duker JS, Izatt JA, Swanson EA, Fujimoto JG: Imaging of macular diseases with optical coherence tomography. Ophthalmology 120:217-229, 1995
9. Drexler W, Hitzenberger CK, Sattmann H, Fercher AF: Measurement of the thickness of fundus layers by partial

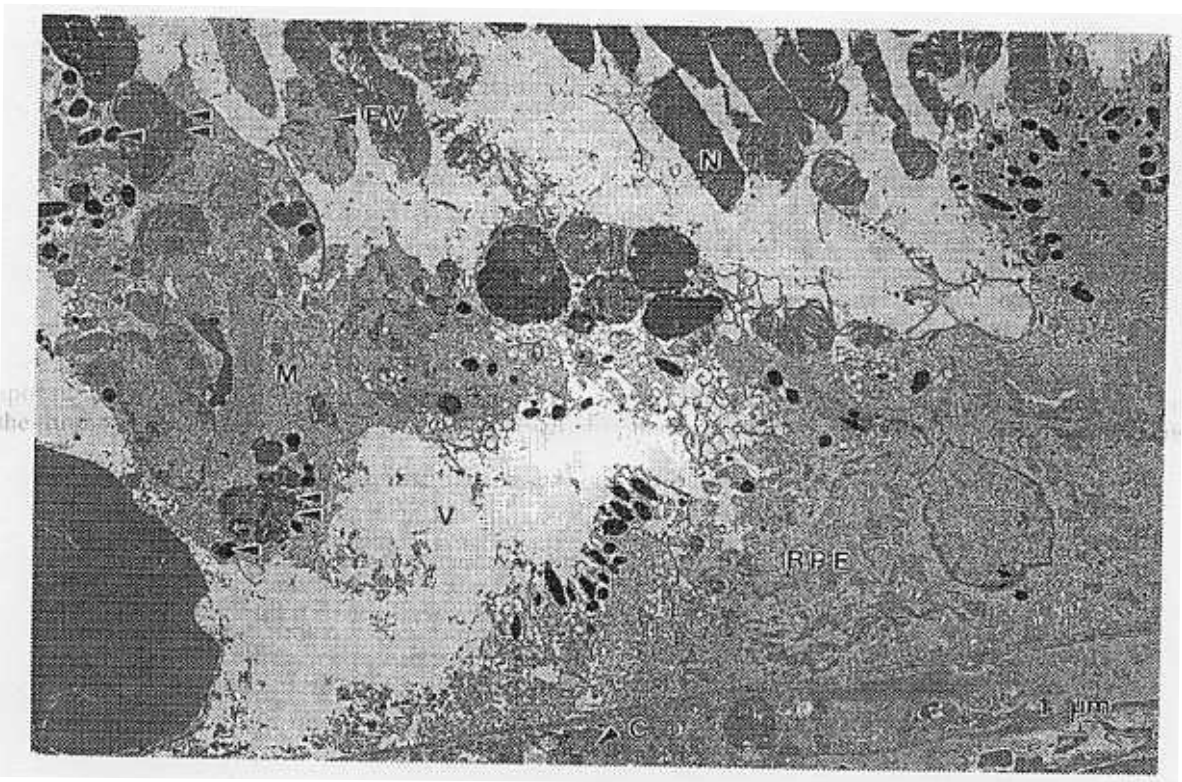

Fig. 13c.

Fig. 13. TEM micrographs through: *13a.* the control tissue; *13b.* the center of the large IR lesion in Figure 3; and *13c.* the center of the central argon lesion in Figure 3.

Comparing the pathology of the argon and IR retinal lesions at 48 hours postexposure (Figs. 10 to 13), reveals that the argon lesions show more RPE involvement than the IR lesions, but that photoreceptor nuclear involvement was greater with the IR exposures. Inner nuclear layer response was also greater in the IR lesions. Further, the pronounced inflammatory reaction observed at the vitreous-ILM interface suggests that the IR exposures induced more inner retinal effects. All these observations emphasize that the gradual tissue absorption of the IR radiation results in involvement of the full retinal thickness.

The argon marker lesions seen in Figures 3 to 6 were induced by exposures much higher than the threshold dose required to produce a minimal visible lesion. At threshold, the argon lesion would be ~20-30 μm in diameter and the damage confined primarily to the RPE layer[14] where the greatest part of the absorption occurs. Only as the exposure does is increased above threshold does the thermal conduction away from the highly absorbing RPE layer result in damage to more distal retinal and choroidal tissues. In contrast, the 1.318-μm lesion at threshold (*i.e.*, at the lowest exposure does which produces an ophthalmoscopically detectable lesion) is already several hundred microns in diameter, in part because chromatic aberrations at this wavelength yield a much larger image diameter at the retina. And, as indicated above, the threshold IR lesions involves the full thickness of the retina. ICG angiography and the pathological evaluation also indicate minor choroidal involvement.

The 1.318-μm retinal effect also differs from thermal damage following visible-wavelength laser exposures, both in the long delay times before ophthalmoscopically visible lesions are first observed and in the late progressive effects which have been detected. Visible-wavelength laser-in-

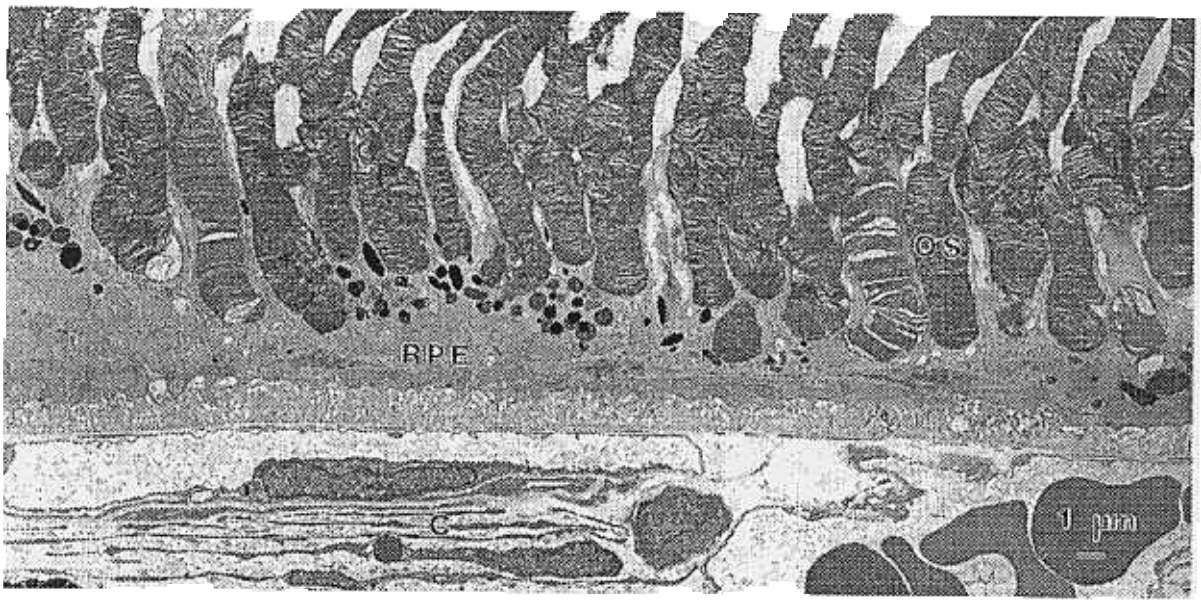

Fig. 13a.

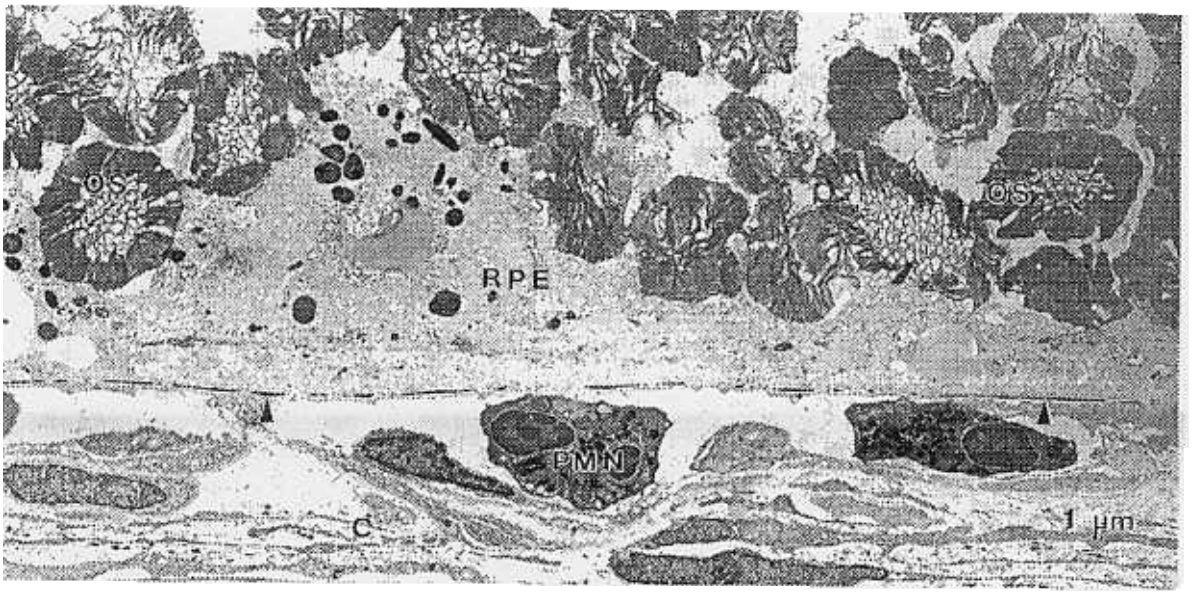

Fig. 13b.

see Fig. 9) involving the retinal lesion and adjacent vitreous.

With 1.318-µm exposure doses sufficient to induce funduscopically visible retinal lesions, both SLO and OCT imaging indicate involvement of the inner retina. But stepping through the retinal layers with the SLO shows that the lesions are largest and most readily detected in the *outer retina* (Fig. 6). Pathological evaluation shows that the 1.318-µm lesions are centered in the ONL.

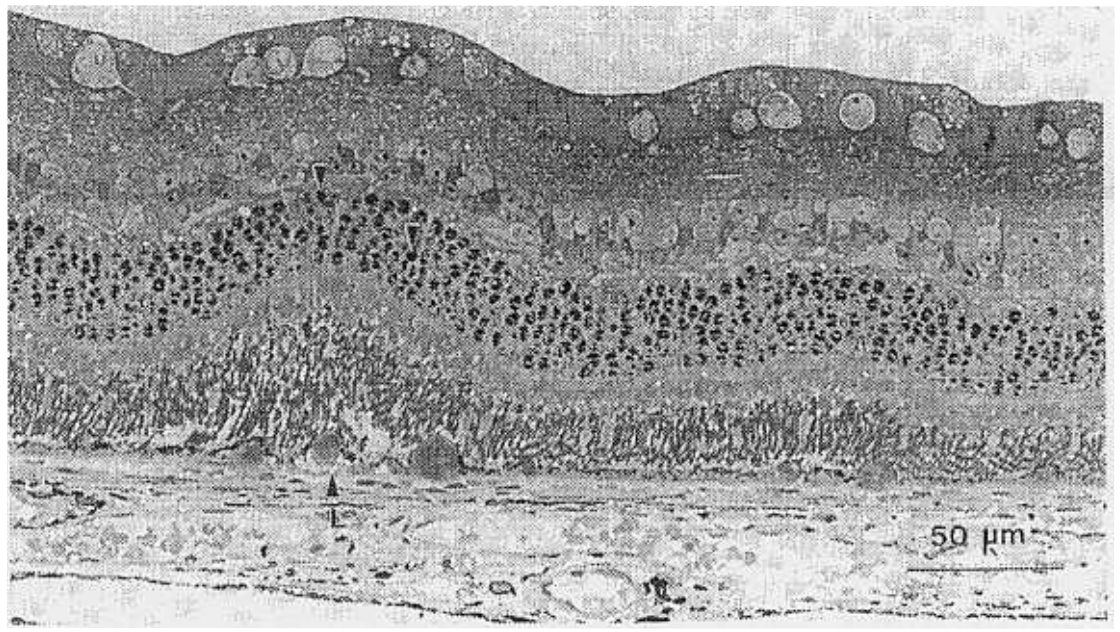

a

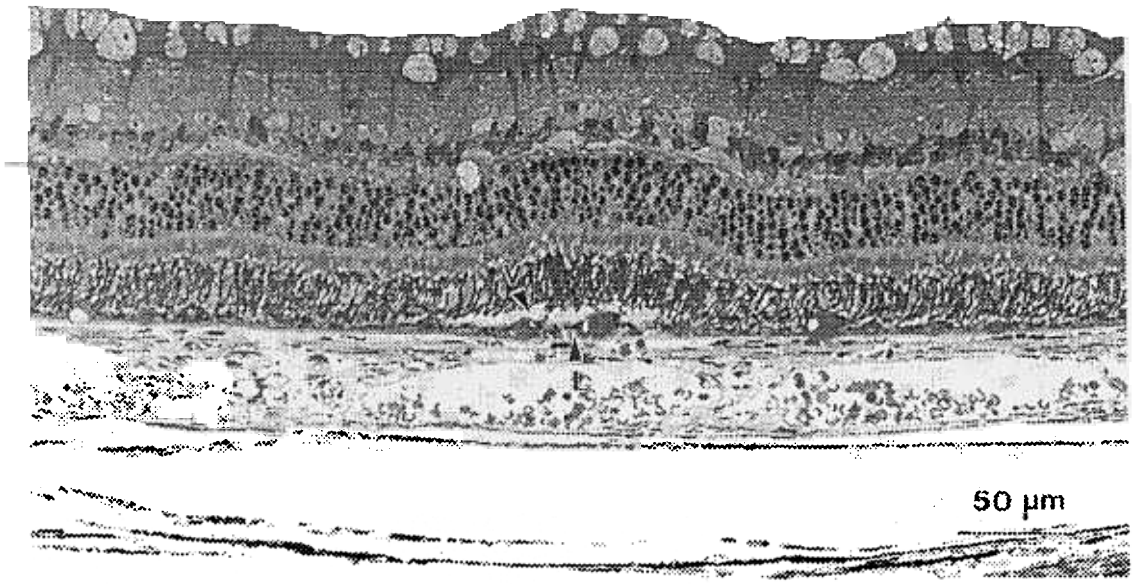

b

Fig. 12. Light micrographs through the centers of the IR lesions in the same eye as that seen in Figure 3, but at exposure sites at which lesions were not ophthalmoscopically visible (see text).

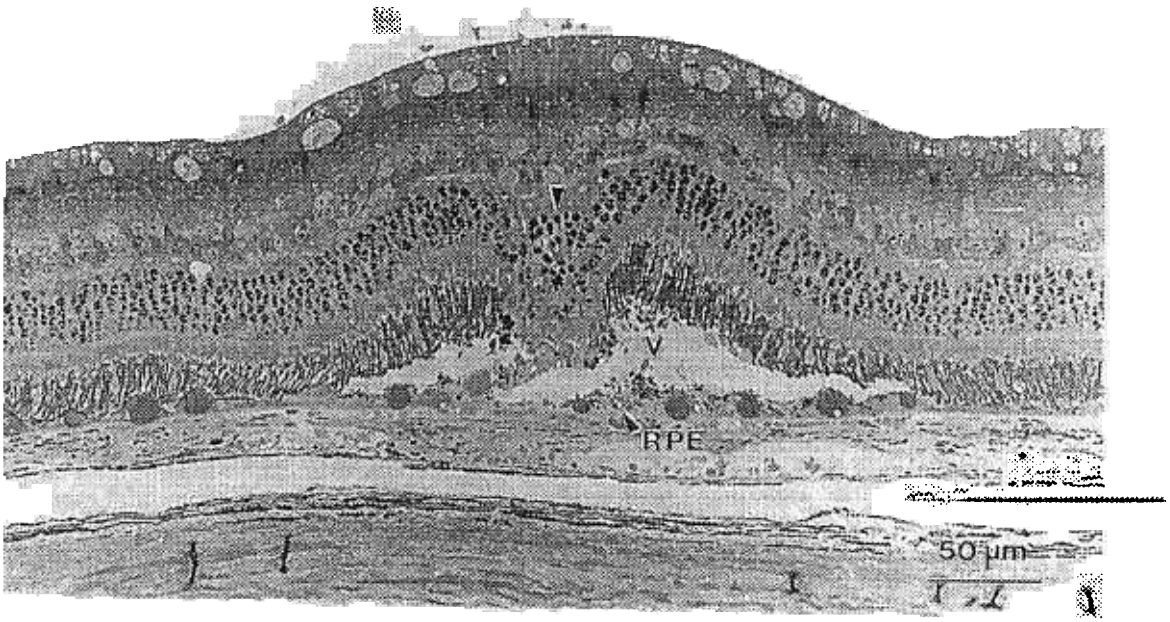

a

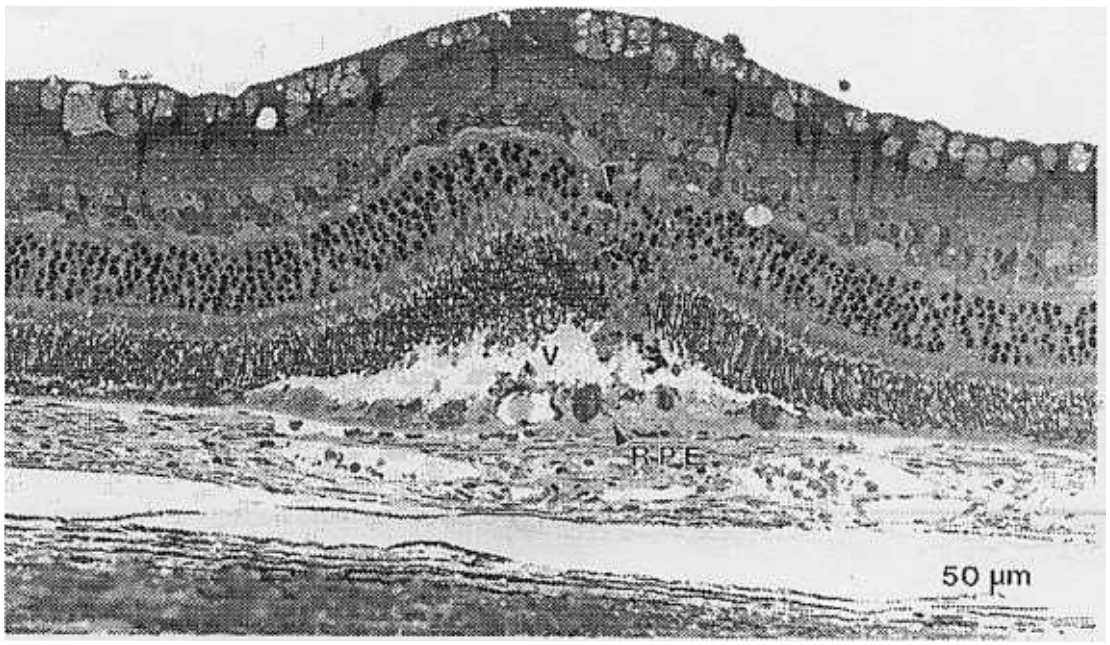

b

Fig. 11. Light micrographs through the centers of the argon marker lesions shown in Figure 3. *11a.* Center marker lesion; *11b.* right-hand marker lesion.

Retinal pathology

Figures 10a and 10b are light micrographs through the centers of the two IR lesions seen in Figure 3. The ocular tissues were fixed at ~48 hours postexposure. Figure 10a corresponds to the larger ophthalmoscopic lesion but, in fact, the two exposure sites received equal doses of IR radiation. Injury appears to be centered in the ONL. Photoreceptor inner and outer segments (IS and OS, respectively) both show degenerative changes. OSs are separated about halfway along their length, and the OS tips are embedded in the apical portions of the RPE. Inflammatory cells (arrows) are present in the vitreous close to the ILM. Some nuclei in the inner nuclear layer (INL) stain dark, but involvement is much less than in the ONL. The large subretinal vacuoles (V) (typical for suprathreshold laser-induced retinal lesions) are produced by RPE swelling and edema, although they may be exaggerated by additional artifactual separation. (Note that this type of artifact would not be present in the OCT image.) From Figure 10b, it appears that some of the vitreous inflammatory cells are adherent to the ILM and that some OSs are attached to the RPE near the lesion center.

Figures 11a and 11b are light micrographs through the centers of the central and right-hand argon lesions seen in Figure 3. Photoreceptors have darkly stained nuclei (arrows) and show degenerative changes along their full length. The amount of RPE swelling is much greater than in the IR lesions, and vacuoles are apparent in the subretinal space. OS tips are not attached to the RPE apical processes. There are very few inflammatory cells in the vitreous above the lesions. Instead, more macrophages are observed in the subretinal space than were found at IR lesion sites.

Figures 12a and 12b are light micrographs taken near the centers of two lower dose IR exposure sites. Lesions (L) at these sites were visualized only with 0.780-μm SLO observation (Fig. 6). The only evidence of degenerative change at 48 hours postexposure are the few dark nuclei in the ONL (arrows), the slight vacuolization in the RPE, and slight swelling in the inner retina.

Figures 13a, 13b and 13c are TEM micrographs showing control retina, the center of the larger IR lesion seen in Figure 3, and the center of the central argon lesion seen in Figure 3, respectively. The control retina (Fig. 13a) illustrates normal OS, IS, RPE, and choroid. In the center of the IR lesion (Fig. 13b), OSs have rounded up, *i.e.*, outer portions of broken OSs have formed circular profiles with vacuolated membranes found in the centers. The RPE appears to be missing some melanin granules, and the cytoplasm is edematous and lightly stained, but intact. Bruch's membrane shows an increased lamellar density (arrows). Polymorphonuclear leukocytes (PMNs) are present in the choroidal vasculature, which is not congested.

Figure 13c, taken through the center of the argon lesion shows OSs with a finer vesiculation (FV) or none at all. Large macrophages (M) are seen engulfing outer segment debris (double arrows) and melanin granules (arrows). The RPE shows more extensive vacuolization than in the IR lesions and the underlying choroidal vessels show congestion (C).

Discussion

The results demonstrate both the unique nature of the IR-laser-induced ocular damage and the power of the SLO and OCT techniques in detecting such damage and differentiating the effects within the various layers of the ocular medium and retina/choroid. Noteworthy is the fact that the SLO was able to *detect IR-induced lesions in the retina* (Fig. 6) even when the exposure dose was below that which yielded lesions detectable by fundus camera observation. Also of interest is the OCT image revealing the path of the 1.318-μm laser beam through the aqueous humor at two months postexposure (Fig. 8). The 'track' is clearly seen to be in line with the corneal and lens lesions induced by the 1.318-μm exposure, *and is prominent even when the imaging beam is not aligned with normal incidence to the corneal and lens surfaces. This latter observation differentiates the aqueous scattering from OCT artifact usually associated with specular reflection. There may be an analogy between the secondary aqueous reaction (visualized between the corneal and lens lesions) and the delayed inflammatory response (also noted at two months postexposure;*

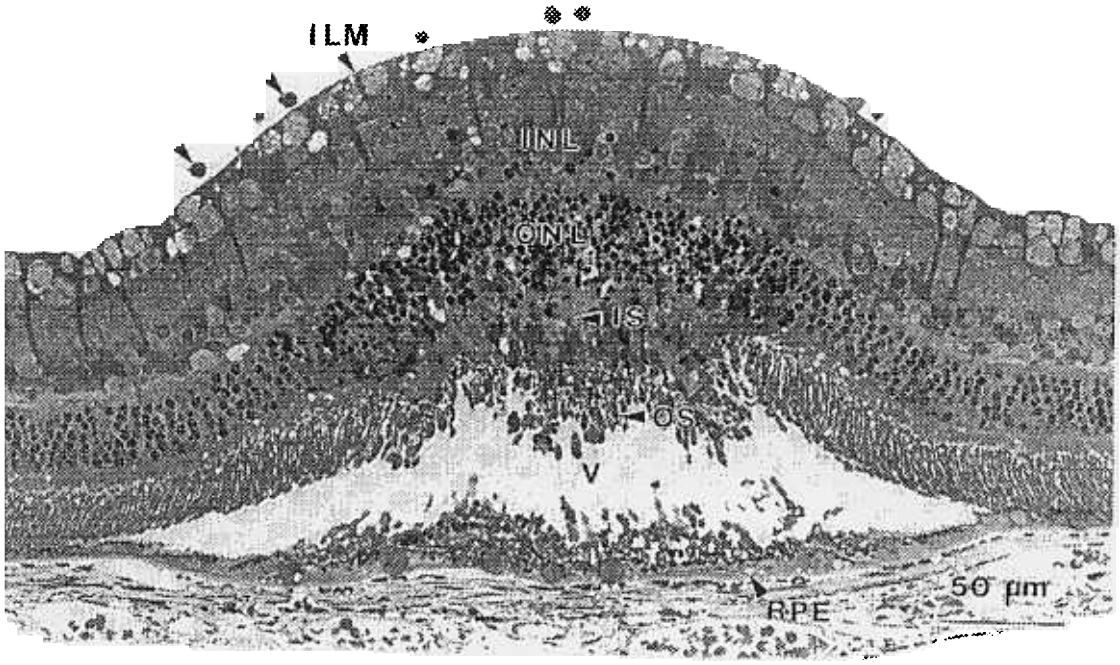

a

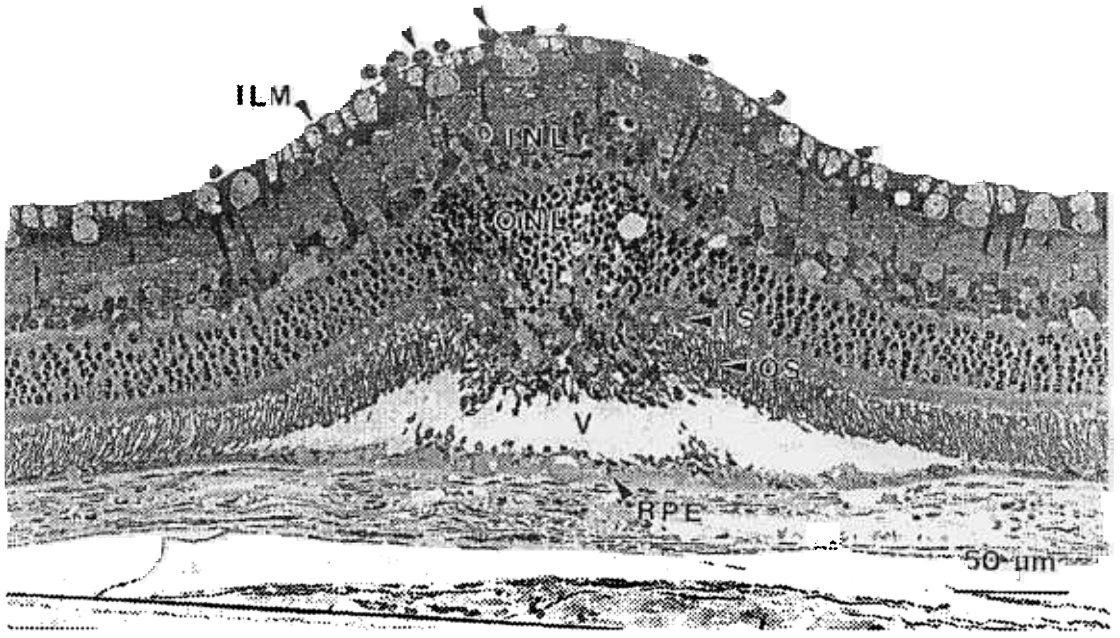

b

Fig. 10. Light micrographs through the centers of the IR lesions shown in Figure 3. *10a.* Larger of the two IR lesions; *10b.* smaller (right hand) of the two IR lesions. The tissue was fixed at 48 hours following laser exposures.

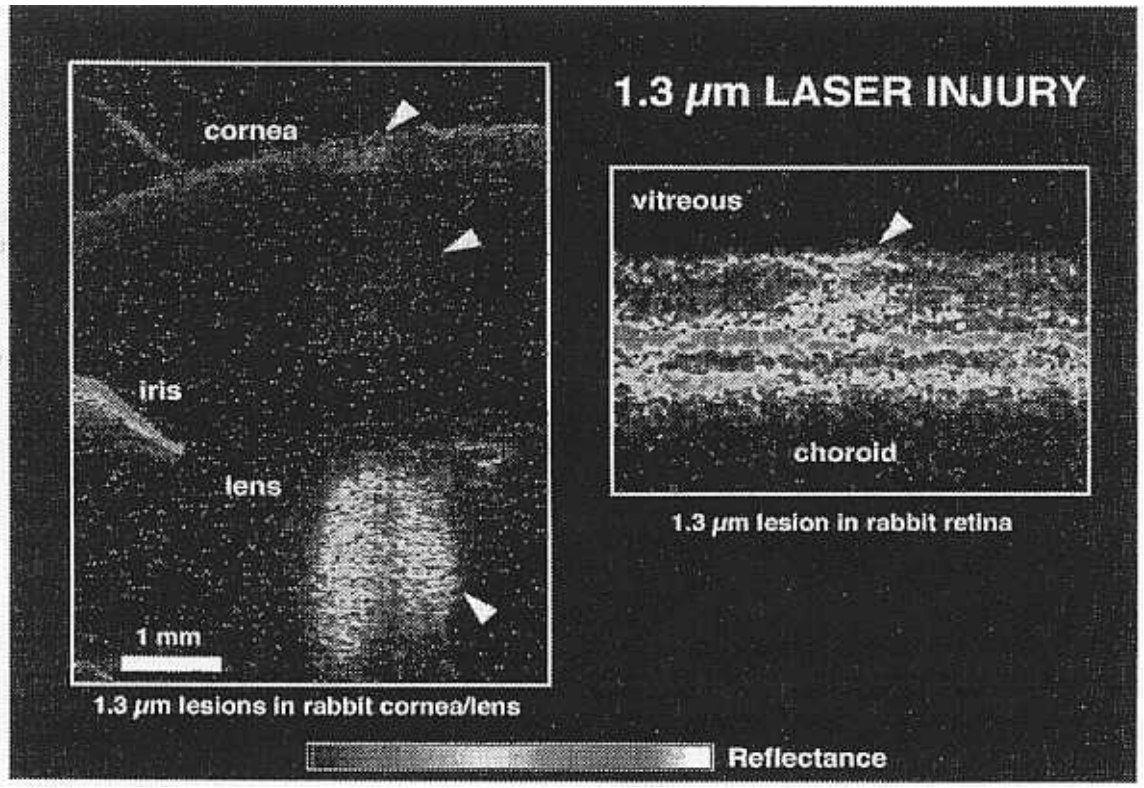

Fig. 8. OCT images, taken at two months postexposure, illustrating 1.318-μm anterior chamber lesions (left panel) and a retinal lesion (right panel) in the same eye, with all the lesions induced by the same exposure.

hours postexposure (Fig. 7). The OPL/ONL damage is similar in appearance to that observed at 24 hours postexposure, while the deeper retinal layers remain relatively unaffected. This OCT image is to be reconciled with the funduscopic appearance of the lesion at two months postexposure, shown in Figure 9. Whereas the 24-hour postexposure fundus camera observation revealed an ~500-μm circular lesion and that appearance was stable with several viewings over the next ten days, by two-months postexposure, the effect had progressed to the large (~1 mm) irregularly shaped lesion seen in Figure 9. This irregularly shaped lesion which, upon funduscopic and SLO observations, appeared to involve the anterior retina, slowly dispersed so that by three months postexposure the underlying circular lesion was again revealed.

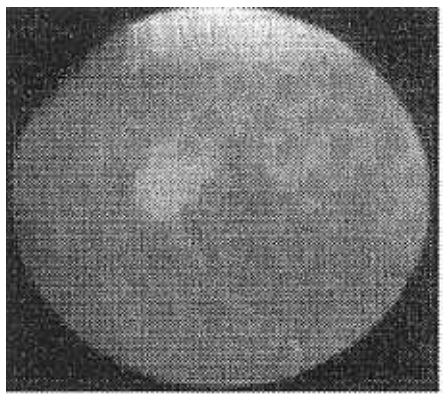

Fig. 9. Fundus photograph, taken at two months postexposure, of the same eye as that seen in Figure 8, illustrating the large (~1 mm), irregularly shaped retinal lesion which had developed at the site of a 1.318-μm laser exposure.

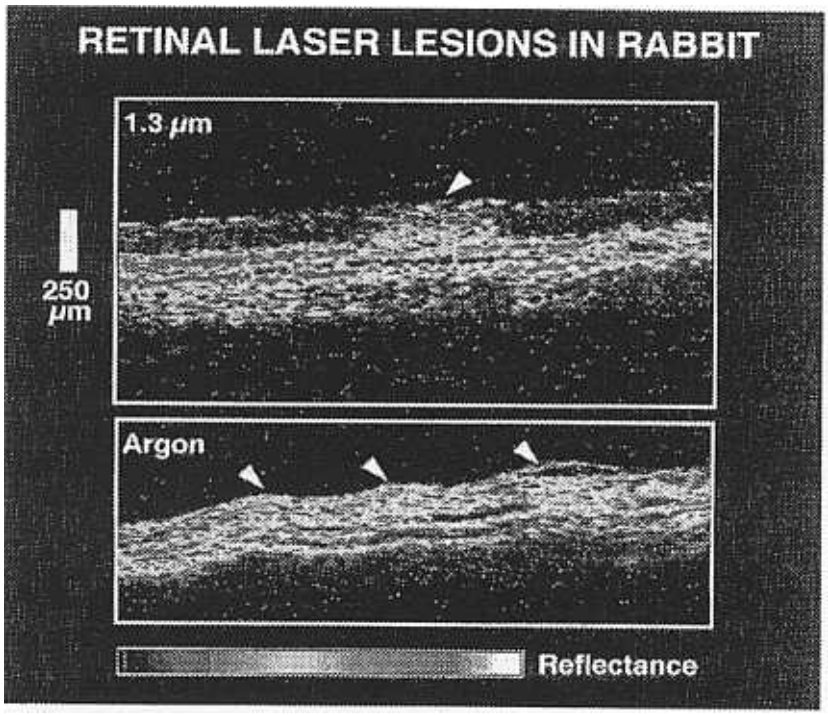

Fig. 7. OCT images comparing a 1.318-μm retinal lesion (upper panel) to three 0.514-μm lesions in the same eye (lower panel). The images were taken at 24 hours following laser exposures.

Several retinal features are explicitly visualized in the OCT images, including *the outer plexiform layer (OPL) and the retinal pigment epithelium (RPE)/choroid interface, which appear as the upper and lower highly scattering red layers, respectively.* Below the RPE, the backscatter signal is gradually attenuated as one moves deeper into the choroid. The inner-limiting membrane (ILM) of the retina is clearly delineated from the vitreous humor. Normal retina is found at the right and left borders of the images.

The 1.318-μm-induced damage seen in Figure 7 (upper panel) is pronounced in the OPL and the adjacent outer nuclear layer (ONL). There is also a noticeable increase in backscatter throughout the inner retinal layers. In contrast, the argon lesions (bottom panel), exhibit more extensive damage in the deeper retinal layers including the RPE and choroid. In all three argon lesions, elevation of the retina is observed, possibly due to the rapid heating and vacuolization within the retina. The right-most lesion also shows a vacuole below the ILM, involving the NFL and ganglion cell layers.

Figure 8 shows OCT images acquired from the anterior chamber (left panel) and retina (right panel) of an eye which, two months earlier, had received a 2 W, ~10-second exposure to the 1.318-μm Nd:YAG laser. Thus, the exposure dose is comparable to those which induced the IR lesions seen in Figures 3-6 but, in this instance, the laser beam diameter incident at the cornea was ~1 mm instead of 5 mm. *As a result of the higher irradiance level incident at the eye, corneal and lenticular lesions were induced in addition to the retinal lesion.* Slit-lamp and fundus camera photographs of these lesions have been published in an earlier report[3].

The corneal and lenticular lesions are visualized in the left panel of Figure 8. Significant opacification is indicated in the nuclear region of the lens, while relatively minor damage is seen in the cornea. The path of the laser beam through the aqueous humor is visualized, although this opacification is also minor.

The retinal image of Figure 8 indicates that, at two months postexposure, the disruption of the inner retinal layers is more pronounced than at 24

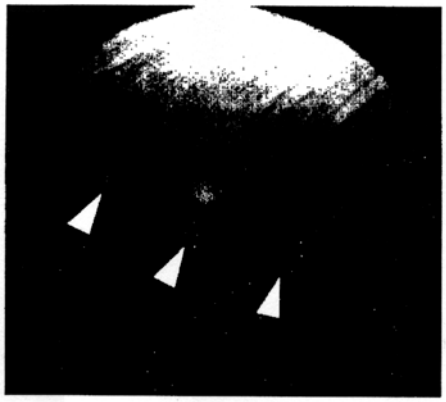

Fig. 3. fundus photograph showing IR (1.318 μm) and argon (0.514 μm) laser-induced lesions in the rabbit eye. *Arrows indicate the three argon marker lesions.* The photograph was taken 24 hours after laser exposures.

Fig. 5. SLO image (20° field of view) taken with the same viewing conditions as for Figure 4, but with confocal slice moved in the anterior direction to visualize the nerve fiber layer.

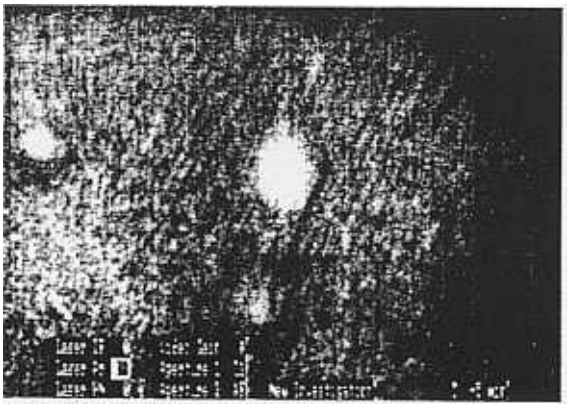

Fig. 4. SLO image (40° field of view) of the same eye as that seen in Figure 3 taken with 0.488-μm illumination and using the smallest confocal aperture. The image was taken at 24 hours following laser exposures.

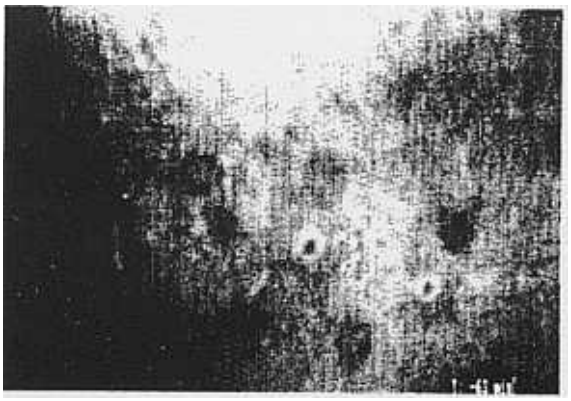

Fig. 6. SLO image (40° field of view) taken with 0.780-μm illumination, but with other viewing conditions the same as for Figure 4.

exposure showed leakage at the argon lesion sites, but not elsewhere. The filling pattern indicated some blockage of retinal vessels across the area between the two argon and two IR lesions in Figure 3. ICG angiography showed choroidal blockage and diffuse staining at the IR exposure sites.

Optical coherence tomography

OCT images through the centers of retinal lesions induced by 0.514- and 1.318-μm laser radiation are shown in Figure 7. The OCT images were also taken at 24 hours postexposure, and laser exposure doses were comparable to those which produced the funduscopically visible lesions seen in Figures 3-6. The top panel of Figure 7 is an image through a 1.318-μm lesion (arrow). The bottom panel is a cut through three adjacent argon lesions (arrows). The color bar under the images scales the intensity of tissue backscatter. The red/white end of the scale represents the highest backscattering, while the blue/black end is associated with the lowest backscattering.

nologies image-processing system, and printed. SLO examinations generally included fluorescein and indocyanine green (ICG) angiographies. The former allowed evaluation of retinal vascular leakage and blockage from lesion sites in the sensory retina, while the ICG angiography was used to detect blockage in the choroidal blood supply.

The OCT instrument utilized a modified ophthalmic slit-lamp to image *in vivo* ocular structures of *two rabbit subjects*. The subjects contained a variety of corneal, lens, and retinal lesions induced by the 1.318-μm Nd:YAG laser[3], as well as retinal lesions induced by the argon laser. The light source for the OCT interferometer was an 830-nm super-luminescent diode laser that enabled imaging with an incident optical power of 200 μW. Images were acquired either vertically or horizontally (as viewed with the slit-lamp) through selected lesions. The instrument achieves a spatial resolution at the retina of ~15 μm in both the longitudinal and transverse directions.

Two rabbits selected for pathological evaluation were euthanized with an overdose of Nembutal. The retinas were processed for routine transmission electron microscopy (TEM)[12]. Briefly, both eyes were enucleated and immersion-fixed within five minutes of death with a cacodylate-buffered solution (4°C) containing 1% glutaraldehyde and 1% paraformaldehyde[13]. Approximately 24 hours later, strips of retina (~2x4 mm) containing the laser-induced lesions were dissected out for further processing. Plastic sections of 1-μm thickness were first examined by light microscopy to determine lesion centers. Then, thin sections for electron microscopy were cut through the lesion centers, using a diamond knife. The thin sections were stained with uranyl acetate and lead citrate, and then examined and photographed with a Zeiss TEM at 60 kV.

Results

Figure 3 is a fundus photograph illustrating retinal lesions induced in the rabbit eye by 0.514- and 1.318-μm laser radiation. The photograph, taken at 24 hours postexposure, *shows three argon-laser-induced marker lesions (arrows) and two IR-laser-induced lesions directly above the central and right-hand marker lesions.* The marker lesions are ~200 μm in diameter and were visible immediately following exposure. The IR lesions were not funduscopically visible on the day of exposure. By 24 hours postexposure, the IR lesions were readily detected with the fundus camera and, as seen in Figure 3, were larger and more reflective than the argon marker lesions. The IR lesions developed somewhat further in size and reflectivity during the ensuing 24-hour period, but beyond 48 hours postexposure, the appearance of the lesions stabilized.

Scanning laser ophthalmoscopy

SLO observations on the eye seen in Figure 3 also failed to visualize the IR lesions on the day of exposure. By 24 hours postexposure, the two IR lesions were apparent with all illuminating wavelengths of the SLO. Figure 4 is an SLO image, at 24 hours postexposure, using 0.488-μm illumination. The smallest confocal aperture (C1) was used, and *the confocal slice (-1.9 D) lies in the inner retina but below the nerve fiber layer (NFL). In this image, both the argon and IR lesions have appearances similar to those seen with normal fundus camera viewing* (Fig. 3). Figure 5 shows a 0.488-μm image of the same eye, but with the confocal plane moved in the anterior direction into the NFL. Intact NFL fibers are imaged over both the argon and IR lesions.

Figure 6 shows an SLO image of the same eye using 0.780-μm illumination, but with all other viewing conditions as in Figure 4. With 0.780-μm illumination, the image is moved deeper into the retina. The argon lesions at this plane are the same size as in Figure 4, but exhibit dark central areas. The IR lesions are considerably larger and more diffuse. Further, several additional IR lesions are now detected. *The additional IR lesions are seen at sites directly* below and in between the argon marker lesions, *and resulted from exposure doses ranging from ~0.25 to 1.0 times the dose required to induce the IR lesions visible in Figures 3 and 4.* These additional lesions were not visualized with the SLO imaging wavelengths other than 0.780 μm, nor with the white light fundus camera illumination.

Fluorescein angiography at 24 hours post-

non-invasive, *in situ* observations of ocular tissues and, specifically, to detect laser-induced retinal effects. The imaging techniques allow *repeated post-exposure examinations of the progression of damage, potentially yielding a more detailed interpretation* of the laser-tissue interaction and the subsequent tissue reactions than does the static picture(s) captured by pathological evaluation.

While the SLO approach is relatively well established, use of a confocal aperture in the SLO apparatus has not been widely applied[4,5]. The confocal aperture effectively allows adjustment of the depth of the imaged confocal slice within the eye. Coupled with the use of any of several illuminating wavelengths, this technique allows visualization of discrete retinal layers and affords the opportunity to detect differential damage effects within those layers.

OCT is a new imaging modality that permits high-resolution, cross-sectional tomographic imaging of the architectural morphology of biological tissues *in vivo*[6]. Imaging is performed by directing a focused light beam into the tissue *and using low-coherence interferometry to measure the delay time (echo delay) for the backscattered light to return to the instrument. In contrast* to the end-face view provided by slit-lamp and funduscopic observations, OCT permits the imaging of ocular structures from the cross-sectional perspective. The clinical diagnostic potential of OCT has been demonstrated in the transparent tissue of the eye[7-9], as well as in highly scattering tissue[10,11].

Methods

The experimental subjects were *15 Dutch Belted rabbits* (*Oryctolagus cuniculus*). Animals used in this study were procured, maintained, and used in accordance with the Animal Welfare Act and the "Guide for the Care and Use of Laboratory Animals" prepared by the Institute of Laboratory Animal Resources, National Research Council; and the ARVO Resolution on the Use of Animals in Research. All experiments used appropriate levels of anesthesia *(IM injection of ketamine (20 mg/kg) mixed with xylazine (0.5-1.0 mg/kg))*, so the subjects did not experience pain or distress.

Pre-exposure screening of subjects to ensure clear ocular media and normal ocular tissues generally consisted of a slit-lamp examination, a fundus camera examination, fluorescein angiography, baseline photography taken while the subject was still in position at the fundus camera, and refraction to the nearest 0.25 diopter.

Ocular exposures were made with a cw Nd:YAG laser equipped with a pair of mirrors to optimize the output at 1.318 μm. An intracavity etalon was used to select the wavelength of interest while suppressing other Nd:YAG emission lines. The laser beam was directed through a 0.5-m scanning monochromator to a germanium photodiode to ensure that the selected wavelength was free of contaminating laser emissions. CW output was stable at a maximum level of ~2 W. An electronically controlled mechanical shutter was used to select the exposure duration, which was the variable for ocular threshold determinations. Beam profiles were determined using a 2-D laser beam analyzer. Marker lesions were produced on the subjects' retinas with an air-cooled argon-ion laser with a cw power of 60 mW and an exposure duration of 15 msec. Elsewhere, we have reported corneal, lens, and retinal thresholds in both rabbits and primates for 1.318- and 1.356-μm radiation obtained from the Nd:YAG laser[3]. The SLO and OCT observations discussed in this paper, as well as the pathological evaluations, were conducted only in rabbits and only for one IR wavelength (1.318 μm) and one visible wavelength (0.514 μm).

IR laser exposure times ranged from one to ten seconds. The 1.318-μm collimated beam was ~5 mm in diameter when incident at the cornea. This yielded exposure doses of ~10-100 J/cm^2 at the cornea. Procedures for delivering laser exposures and laser beam diagnostics are described elsewhere[3].

Subjects were examined by standard fundus ophthalmoscopy and SLO immediately following laser exposure, and again at 24 and 48 hours postexposure. The Rodenstock SLO was capable of projecting four wavelengths: argon blue (0.488 μm), argon green (0.514 μm), helium neon (0.633 μm), and gallium arsenide (0.780 μm)[5]. A confocal aperture was employed[4]. Images were recorded on super VHS video tape. Individual video frames were digitized with a Delta Tech-

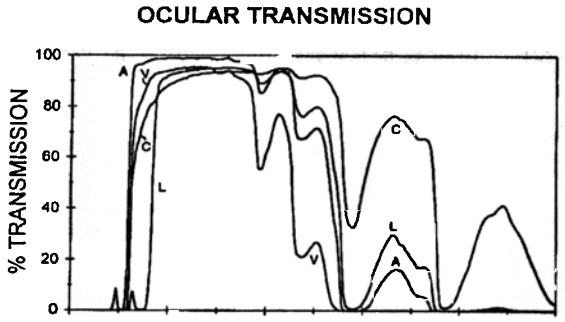

Fig. 1. Transmission spectra of the components of the primate eye. C: cornea; A: aqueous humor; L: lens; V: vitreous humor.

ured along the horizontal axis, as indicated in Figure 2b. Figure 2a remains essentially unchanged if any other visible wavelength is substituted for 0.514 μm.

The solid lines in Figures 2a and 2c show the variation in absorption coefficients as one moves through the ocular medium[1]. Using these absorption coefficients and treating each ocular component as homogeneous, the percent of corneal incident radiation reaching any given depth into the ocular medium is calculated and shown by the dotted curves in Figures 2a and 2c. At 0.514 μm, most of the corneal incident radiation reaches the retina, but at 1.318 μm, the transmission to the retina is ≤5%. Taking the focusing power of the eye into account, the relative laser irradiance at any point along the horizontal axis can be approximated, and is plotted as the dashed curves in Figures 2a and 2c. For visible wavelengths, the retinal hazard is readily appreciated from the high irradiance level at the retina, coupled with a high retinal absorption coefficient[2]. At 1.318 μm, on the other hand, the retinal irradiance exceeds that incident at the cornea by a relatively small margin.

In a preliminary report[3], it was shown that exposures in the 'eye-safe' wavelength range can, indeed, result in multiple damage sites throughout the ocular medium and the retina. It was also noted that initially unaffected IR laser exposure sites, when monitored over time, may reveal slowly developing (days or longer) tissue degeneration, and that the tissue degradation may ultimately progress to involve regions surrounding the discrete areas subjected to laser radiation.

In this report, the laser-tissue interaction at

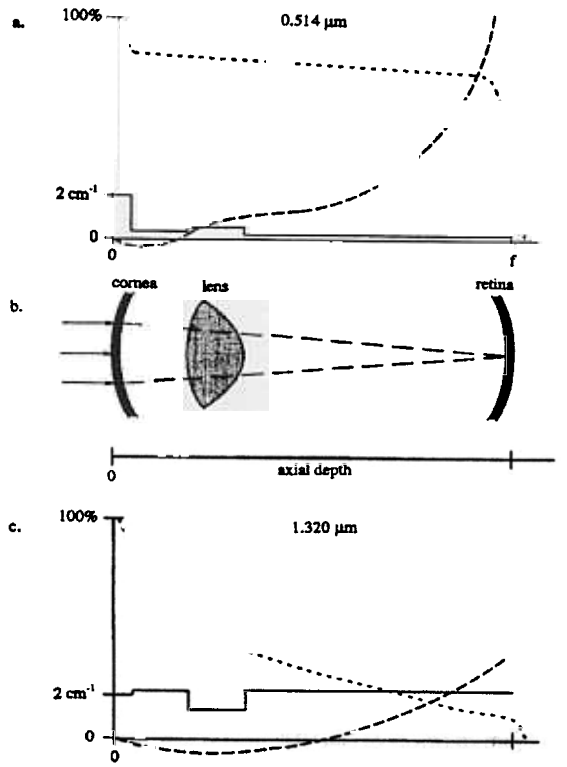

Fig. 2. Schematic depiction of penetration of 0.514-μm and 1.318-μm radiation (*2a* and *2c*, respectively) into an eye of focal length, f (*2b*). The vertical axes of *2a* and *2c* are, in turn, absorption coefficient in cm^{-1} (for the solid lines); percent of corneal incident radiation penetrating to a given depth into the eye (dotted lines); and relative irradiance at a given depth (dashed lines). *The relative irradiance is set equal to 1.0 at the corneal surface.*

1.318 μm is further characterized via *confocal* scanning laser ophthalmoscopy (SLO) and optical coherence tomography (OCT), as well as by examining the associated retinal pathology. For both the imaging approaches and the ocular pathology, the findings in IR laser-exposed retinal tissues are contrasted to those in argon laser-exposed tissues. The SLO and OCT imaging techniques are briefly described below.

Background

Two imaging technologies (SLO and OCT) which employ coherent light sources are applied to yield